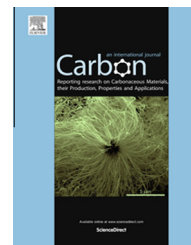


Available at [www.sciencedirect.com](http://www.sciencedirect.com)

ScienceDirect

journal homepage: [www.elsevier.com/locate/carbon](http://www.elsevier.com/locate/carbon)

# Preparation of functionalized water-soluble photoluminescent carbon quantum dots from petroleum coke



Mingbo Wu <sup>a,\*</sup>, Yue Wang <sup>a</sup>, Wenting Wu <sup>a</sup>, Chao Hu <sup>b</sup>, Xiuna Wang <sup>b</sup>,  
Jingtang Zheng <sup>a</sup>, Zhongtao Li <sup>a</sup>, Bo Jiang <sup>a</sup>, Jieshan Qiu <sup>b,\*</sup>

<sup>a</sup> State Key Laboratory of Heavy Oil Processing, China University of Petroleum, Qingdao 266580, PR China

<sup>b</sup> State Key Laboratory of Fine Chemicals, School of Chemical Engineering, Dalian University of Technology, Dalian 116024, PR China

## ARTICLE INFO

### Article history:

Received 9 May 2014

Accepted 11 July 2014

Available online 18 July 2014

## ABSTRACT

Here we report a new strategy for preparation of water-soluble photoluminescent carbon quantum dots (CQDs) from petroleum coke. Petroleum coke was oxidized first in mixed concentrated  $H_2SO_4$  and  $HNO_3$ , and then functionalized by hydrothermal ammonia treatment. The as-made CQDs and nitrogen-doped CQDs (N-CQDs) were characterized by UV–Vis absorption spectroscopy, fluorescence spectroscopy, transmission electron microscope, atomic force microscope, Raman spectrometer, X-ray powder diffractometer, X-ray photoelectron spectroscopy and Fourier transform infrared spectrometer. The results show that the quantum yield of CQDs increases greatly from 8.7 to 15.8%, and the fluorescent lifetime increases from 3.86 to 6.11 ns after the hydrothermal treatment in ammonia. Moreover, the fluorescent color of N-CQDs can be tuned through the amount of doped nitrogen. Both CQDs and N-CQDs are water-soluble, and have uniform particle distribution, strong luminescence, and highly fluorescent sensitivity to pH in a range of 2.0–12.0. The uniform size distribution and nitrogen-doping of N-CQDs help to lead to high yield of radiative recombination, resulting in improved fluorescence properties. This work offers a simple pathway to produce high quality and enhanced photoluminescent CQDs from petroleum coke.

© 2014 Elsevier Ltd. All rights reserved.

## 1. Introduction

Carbon-based quantum dots (CQDs) were discovered in 2004 while separating single walled carbon nanotubes by etching electrophoresis [1]. It has been found that CQDs with novel optical properties, outstanding biocompatibility and robust chemical inertness are of potential as probes for high-contrast bioimaging and biosensing applications, and CQDs with intense and tunable photoluminescence (PL) and high water

solubility are of special importance in catalysis and energy-related fields. As such, it is necessary to develop novel processes to make high quality CQDs with tuned properties in high yield. Up to now, various carbon precursors including graphite [2–5], graphene oxides [6–10], fullerene [11], carbon fibres [12] and organic carbon sources [13–17], have been used to prepare CQDs. Most carbon precursors mentioned above are relatively expensive, which results in a high preparation cost of CQDs to some degree. Petroleum coke is a by-product

\* Corresponding authors: Fax: +86 532 8698 1787, +86 411 8498 6087.

E-mail addresses: [wumb@upc.edu.cn](mailto:wumb@upc.edu.cn) (M. Wu), [jqiu@dlut.edu.cn](mailto:jqiu@dlut.edu.cn) (J. Qiu).

<http://dx.doi.org/10.1016/j.carbon.2014.07.029>

0008-6223/© 2014 Elsevier Ltd. All rights reserved.

in oil refining process, has high content of carbon and low content of ash, and has been demonstrated to be good starting material for production of porous carbons [18]. Petroleum coke is rich of benzene rings or aromatic domains, which make it possible to prepare high quality CQDs.

In terms of synthesis of CQDs, some methods including the chemical oxidation of candle soot [19], the thermal cracking of organic compounds [20], the microwave-assisted hydrothermal synthesis [21], the rapid plasma pyrolysis of egg [22], the alkali-assisted electrolysis of graphite [23] have been reported. Of these methods, the chemical oxidation is effective, convenient, and easy to scale-up [24,25], nevertheless, it is non-selective in terms of cutting the aromatic carbon framework smaller, this is especially the case for the precise control of the morphology and size distribution of CQDs with high fluorescence [26].

To improve the fluorescent performance of CQDs prepared by chemical oxidation, subsequent modifications or doping are required, which helps to tailor the electronic properties of the concerned CQDs by making use of strong electron-donating or electron-accepting molecules. Surface modification/passivation of CQDs by amine-containing agents via covalent bonding is a commonly used method to improve their PL performance [27,28]. Meanwhile, doping is another widely used approach to tune the PL properties of CQDs. N-doping can effectively enhance the PL emission performance of CQDs by inducing an upward shift of the Fermi level and electrons in the conduction band [29]. N-CQDs show nitrogen-content dependent PL intensities with multicolor [30]. Unfortunately, above mentioned works need complicated procedures or expensive passivating agents, which hinder their wide applications. It is reported that primary amine and carbon–nitrogen bonding can be introduced rapidly and easily to passivate CQDs. Tetsuka et al. [31] demonstrated that the molecular orbital resonance due to the delocalized  $\pi$  orbital of GQDs can be induced by direct bonding primary amino groups to the dots' edges, yielding GQDs with high efficiency of narrow PL. Jin et al. [32] reported that the band gap of graphene quantum dots (GQDs) can be tuned by the charge transfer between amino groups and GQDs, leading to a shifted PL emission.

Here we report the synthesis of nitrogen-doped CQDs (N-CQDs) from petroleum coke by an ultrasonic-assisted chemical oxidation method. Under the combined synergistic effect of  $\text{H}_2\text{SO}_4$ ,  $\text{HNO}_3$  oxidation, and ultrasonic wave energy, petroleum coke with cheap price and stacked graphitic layers has been selectively converted to well-dispersed CQDs. The as-made water-soluble fluorescent CQDs are further functionalized by ammonia under hydrothermal conditions, yielding tuneable PL N-CQDs with uniform size and high quantum yield (QY).

## 2. Experimental

### 2.1. Chemicals and materials

All chemical agents used in the present study were analytical pure, sulfuric acid of 98.0 wt.%, nitric acid of 65.0 wt.%, ammonia of 28.0 wt.%, hydrochloric acid of 37.0 wt.%, and

sodium hydroxide were bought from Sinopharm Chemical Reagent Co. of China, and used without further treatment. Quinine (97.0 wt.%) was purchased from Aladdin Industrial Corporation at Shanghai of China. Inorganic filter membrane (0.22  $\mu\text{m}$ ) and 3500 Da molecular weight cut off (MWCO) dialysis membranes (Amicon Ultra-4, Millipore) were purchased from Shanghai Green Bird Science & Technology Development Co. of China. The water used throughout the experiments was deionized water.

### 2.2. Synthesis and purification of CQDs

Petroleum coke (2.0 g) was added into a mixture of concentrated  $\text{H}_2\text{SO}_4$  (45.0 mL) and  $\text{HNO}_3$  (15.0 mL) in a flask under ultrasonic conditions (KQ-700DE, operated at 700 W) for 2 h, then heated under constant stirring in an oil bath at 120 °C for 12 h in reflux. After the reaction, the mixture was cooled to room temperature (RT), and diluted 10 times with deionized water, and neutralized with ammonia till pH = 7.0. The neutralized mixture was filtered by a filter membrane (0.22  $\mu\text{m}$ ) to remove the larger fractions, yielding a solution containing CQDs that was further dialyzed with 3500 Da MWCO for 72 h to remove the salts and tiny fragments. Finally, a deep yellow CQDs solution was obtained, exhibiting yellow emission under 365 nm UV light.

### 2.3. Synthesis and purification of N-CQDs

The as-made CQDs were treated hydrothermally in ammonia to make N-CQDs. For a typical run, 10 mL of as-made CQDs homogeneously dispersed in water (0.1 mg/mL) was mixed with 3 mL of ammonia in a glass vial, and sonicated for 20 min, yielding a mixture that was transferred to a Teflon lined autoclave and heated at 180 °C for 12 h. After cooling back to RT, the solution was filtered again using a 0.22  $\mu\text{m}$  filter membrane to remove the insoluble larger fragments, yielding a supernatant containing N-CQDs that was heated at 100 °C for 1 h to get rid of excess ammonia. Then, the supernatant was dialyzed by the same procedure mentioned before for treating the CQDs, yielding a light yellow N-CQDs solution with a blue emission excited at 365 nm UV light.

### 2.4. Characterizations

X-ray photoelectron spectroscopy (XPS) was recorded on ESCALAB 250Xi spectrometer equipped with a pre-reduction chamber. The position of the C1s peak (284.5 eV) was used to correct the binding energies for other groups due to the possible charging effect. Fourier transform infrared (FT-IR) spectra were recorded on a Nicolet 6700 spectrometer. Raman spectroscopy was recorded using an  $\text{Ar}^+$  ion laser at 514.5 or 633 nm (Renishaw inVia 2000 Raman microscope, UK). X-ray powder diffraction (XRD) measurement was performed on a PANalytical X-ray Diffractometer (Cu  $K\alpha$  radiation,  $\lambda = 0.15406$  nm, 40 kV, 40 mA). The transmission electron microscopy (TEM) images were obtained by JEOL JEM-2100UHR microscope operated at 200 kV. Field emission scanning electron microscopy (FESEM) images were taken in a Hitachi S-4800 scanning electron microscope operated at 5.0 kV. The height profiles of CQDs and N-CQDs were

investigated by an atomic force microscope (AFM, Nanoscope V D3100, Veeco Instruments, USA). UV–Vis absorption spectra were measured at RT by a UV/Vis spectrophotometer (Gold Spectrumlab 54, Shanghai Lengguang Technology Co. Ltd., China). Fluorescence spectra were measured at RT by a spectrofluorometer (F-97 Pro, Shanghai Lengguang Technology Co. Ltd., China). For the excitation dependent emission spectra and PL excitation (PLE) spectra, a Xe lamp was used as an excitation source. The time decay was measured on a Fluoro Max-4 fluorometer (Horiba Jobin Yvon Inc., France). An excitation wavelength of 405 nm was used and emission was collected at 510 nm of CQDs and 475 nm of N-CQDs, respectively.

### 3. Results and discussion

#### 3.1. Preparation of CQDs and N-CQDs

Fig. 1 is the synthesis schematic of CQDs and N-CQDs derived from petroleum coke. The weight yield of CQDs is about 24.0 wt.% in the chemical oxidation step. The QY of CQDs is about 8.7% (Table S1), which is much higher than most CQDs prepared by traditionally chemical oxidation reported in literature [19,24,25]. The results show that petroleum coke with irregular size and shape distributions (Fig. S1) has been oxidized by the mixture of concentrated nitric acid and sulfuric acid to small CQDs that are rich of oxygen-containing functional groups. Low concentration ammonia in the hydrothermal step functions as a chemical knife to polish the edges of CQDs, and have N atoms anchored on the surface of CQDs [33]. The as-made N-CQDs with hydrophilic groups resulted from the chemical oxidation show an excellent solubility and stability in water and other polar organic solvents such as acetone, DMF and DMSO.

#### 3.2. Physical structure of CQDs and N-CQDs

Fig. 2 is the TEM images of CQDs and N-CQDs, showing clearly that the as-made N-CQDs are quasi-spheres, and dispersed well. N-CQDs have a narrow size distribution centering at ca. 3.0 nm, with an average size of 2.7 nm, which are smaller

than CQDs with a wider size distribution centering at ca. 4.5 nm, and an average size of 5.0 nm. The insets in Fig. 2a and c are the typical HRTEM images of CQDs and N-CQDs, indicating certain crystallinity with a lattice space of 0.332 and 0.334 nm, respectively. Both are in good agreement with the 002 planes of graphite, evidenced in the XRD patterns discussed below [34,35].

Fig. 3a is the AFM image of CQDs with a topographic height in a range of 0.5–4.5 nm (Fig. 3c) and an average height of 1.8 nm (Fig. 3b), suggesting that most CQDs consist of ca. 1–8 graphene layers [36]. The heights of N-CQDs are in a range of 1–10 nm (Fig. 3f), with an average height of 3.7 nm (Fig. 3e), indicative of the presence of graphene-like structures in the N-CQDs [35]. This result is similar to the results of N-CQDs made from other carbon precursors in literature [33,37,38].

XRD is a powerful tool for examining the structure of CQDs. Fig. 4a shows that petroleum coke has a very sharp diffraction peak at  $25.8^\circ$  ( $2\theta$ ), while CQDs and N-CQDs show a broader diffraction peak in the whole range. Both CQDs and N-CQDs show a small sharp peak at  $26.7^\circ$  ( $2\theta$ ), which is a little bit higher than that of petroleum coke. The interlayer spacing (ca. 0.334 nm) in CQDs and N-CQDs are more compact than those in the original petroleum coke (ca. 0.346 nm), which is consistent with the TEM observations (Fig. 2). The smaller interlayer spacing in CQDs and N-CQDs can be attributed to the effective  $\pi$ - $\pi$  stacking of graphene sheets with few structural defects [33]. On the other hand, the formation of hydrogen bonds among the O-containing functional groups at the edges of graphene layers in CQDs and N-CQDs may also help to facilitate the compact stacking of graphene layers [39,40].

Raman spectra of petroleum coke, CQDs, and N-CQDs are shown in Fig. 4b, further demonstrating the defects with unsaturated bonds in CQDs. The peak around  $1600\text{ cm}^{-1}$  (G) corresponds to the  $E_{2g}$  mode of graphite due to the vibration of the  $sp^2$ -bonded carbon atoms in the 2D hexagonal lattice, while the peak around  $1370\text{ cm}^{-1}$  (D) exhibits disorder characteristic due to scattering at the edges. The  $I_D/I_G$  ratio of N-CQDs is 1.20, higher than that of CQDs (0.98) and petroleum coke (0.72). The hydrothermal treatment of CQDs in ammonia

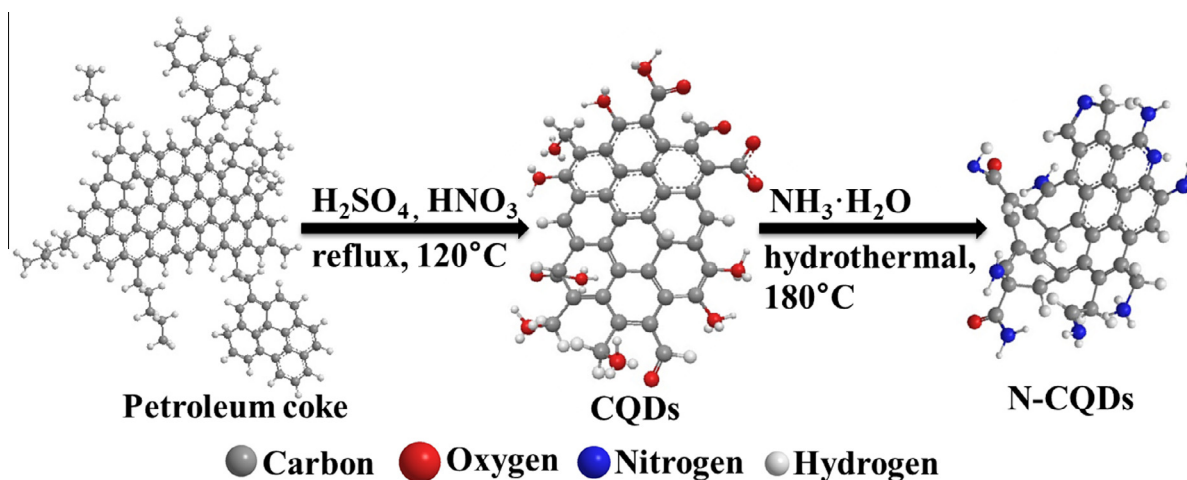


Fig. 1 – Diagram for the preparation of CQDs and N-CQDs from petroleum coke. (A color version of this figure can be viewed online.)

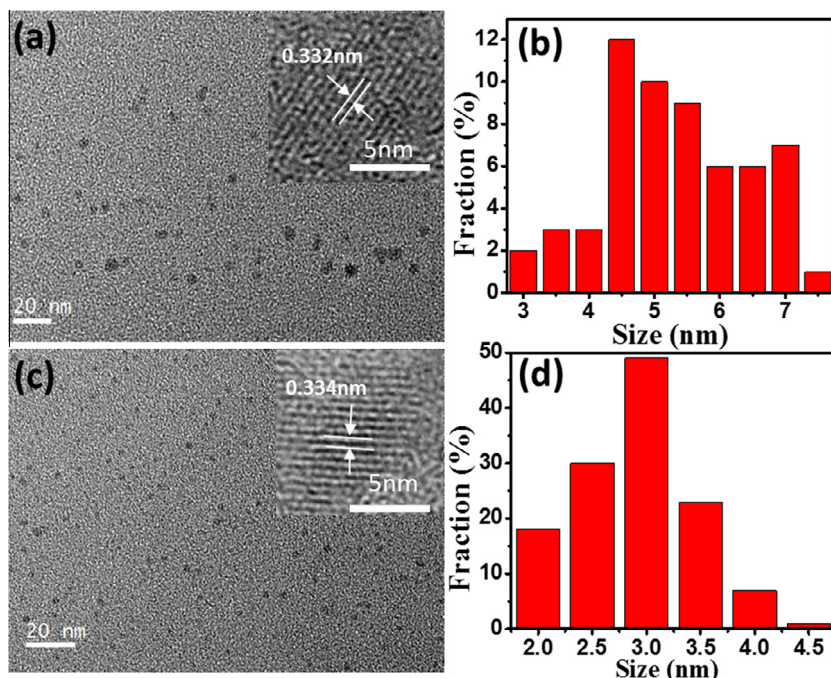


Fig. 2 – TEM, HRTEM (inset) images (a) and the diameter distribution (b) of CQDs. TEM, HRTEM (inset) images (c) and the diameter distribution (d) of N-CQDs. (A color version of this figure can be viewed online.)

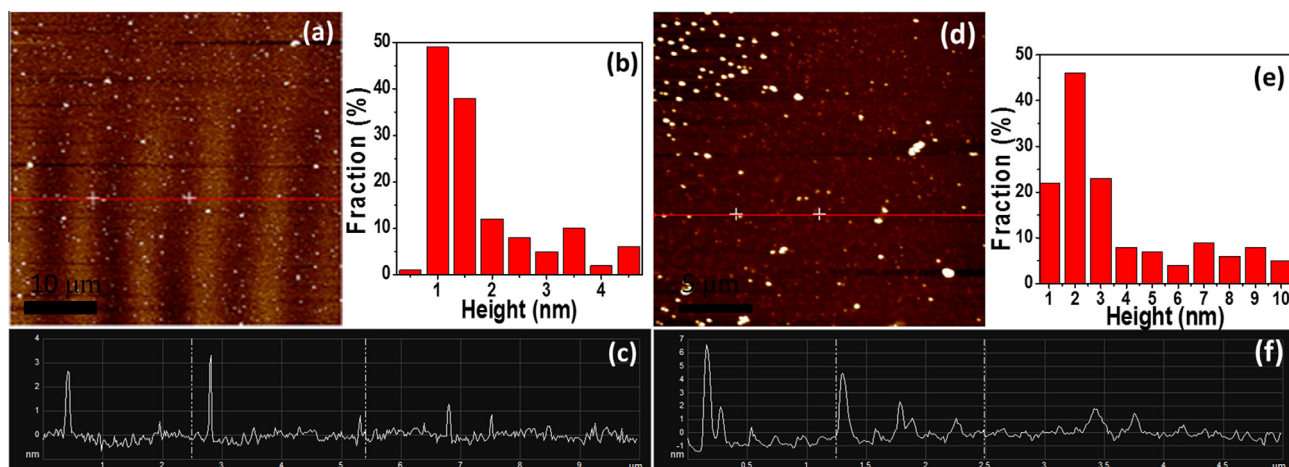


Fig. 3 – AFM image (a), the height distribution (b) and the height profile corresponding to the AFM image (c) of CQDs. AFM image (d), the height distribution (e) and the height profile corresponding to the AFM image (f) of N-CQDs. (A color version of this figure can be viewed online.)

not only cuts  $sp^2$  clusters in graphite sheets into CQDs but also has N atoms anchored to the surface of carbon skeleton, thus, the highest value of  $I_D/I_G$  ratio of N-CQDs may be caused by the increased disorder due to the introduction of C-N bands and amino groups on the surface of N-CQDs [33]. All of the results have suggested that the CQDs derived from petroleum coke are mainly composed of  $sp^2$  graphitic carbons with  $sp^3$  carbon defects and oxygen-rich edges such as hydroxy and carbonyl/carboxylate groups that are abundant on the surface [22]. Raman spectrum of N-CQDs shows a broader D and G bands, suggesting that the intercalation of N atoms into the exterior conjugated carbon backbone has resulted in more disordered structures [31]. In comparison

with petroleum coke, blue shifts of D and G bands in CQDs and N-CQDs can be seen, which is consistent with the results reported before [41].

### 3.3. Chemical structure of CQDs and N-CQDs

The high-resolution C1s XPS spectra of petroleum coke, CQDs, and N-CQDs are shown in Fig. 5a–d. For petroleum coke (Fig. 5a), it has  $sp^2$  C=C bands at 284.9 eV and  $sp^3$  C-C bands at 284.2 eV. The C1s spectrum of CQDs (Fig. 5b) can be resolved as follows [42,43]: C=C/C-C at 284.8 eV, C-O at 285.7 eV, C=O at 288.3 eV and O-C=O at 289.0 eV.

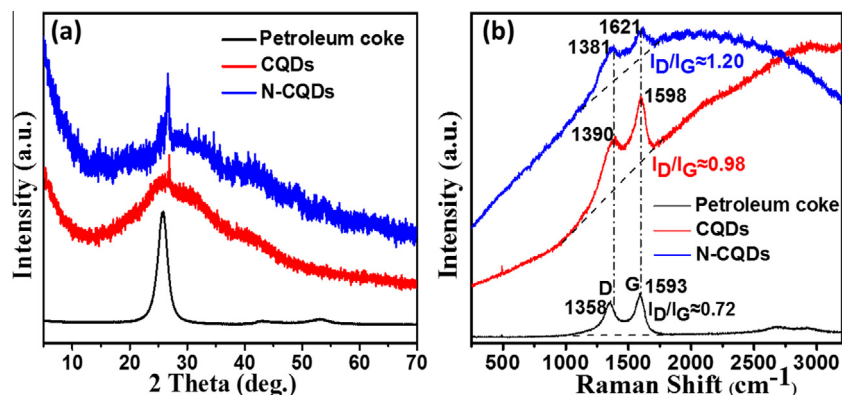


Fig. 4 – XRD patterns (a) and Raman spectra (b) of petroleum coke, CQDs and N-CQDs. (A color version of this figure can be viewed online.)

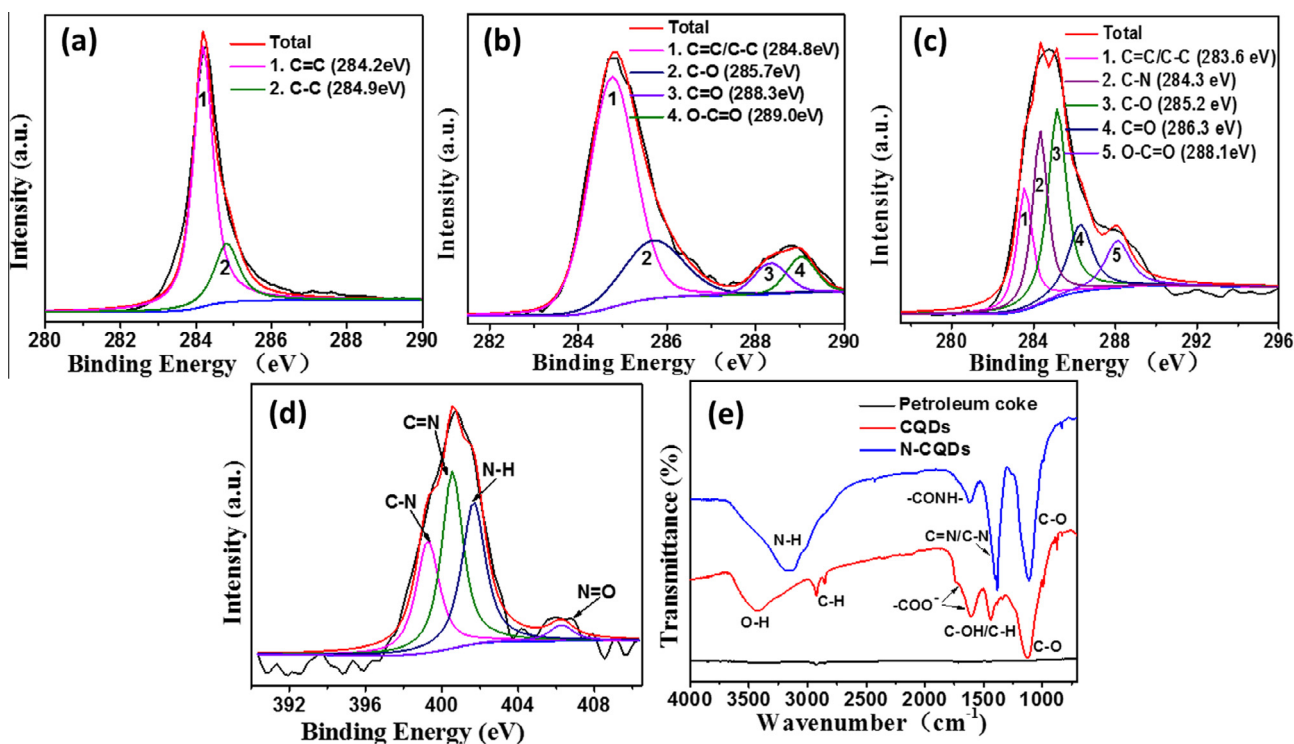
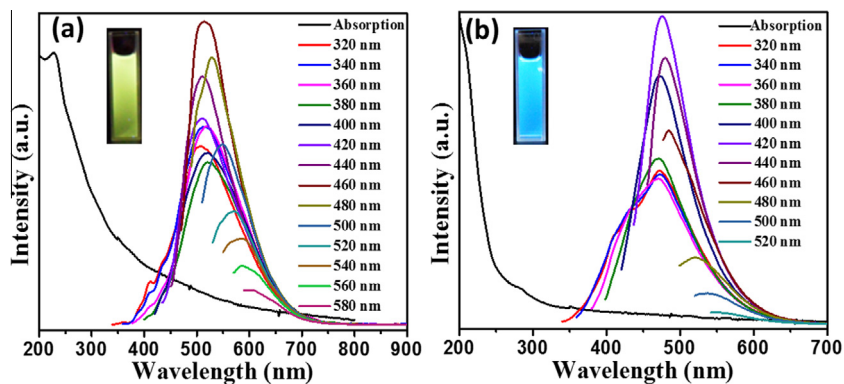


Fig. 5 – High-resolution C1s XPS spectra of petroleum coke (a), CQDs (b), N-CQDs (c), N1s XPS spectrum of N-CQDs (d), and FT-IR spectra (e). (A color version of this figure can be viewed online.)

The full-range XPS spectrum of N-CQDs in Fig. S2 shows N1s peak at ca. 400.7 eV, C1s peak at ca. 284.8 eV and O1s peak at ca. 531.9 eV, the atom contents of which are 7.82, 44.38 and 47.80%, respectively. The existence of N1s confirms the incorporation of N atoms to CQDs in the hydrothermal treatment step in ammonia. As seen in Fig. 5d, the N1s spectrum of N-CQDs has three main peaks centering at 399.3, 400.6 and 401.6 eV, which can be attributed to pyridine-like N, pyrrolic N and N-H, respectively [38,44]. A shoulder peak around 406.3 eV is also observed, which may be due to nitrogen oxides [45]. In addition to C-N bond at 284.3 eV, the high-resolution C1s spectrum of N-CQDs (Fig. 5c) further confirms the presence of oxygen-containing groups [46], such as C-O

(285.2 eV), C=O (286.3 eV) and O-C=O (288.1 eV), which is further confirmed by the FT-IR results discussed below.

The FT-IR spectra of CQDs and N-CQDs are shown in Fig. 5e. The typical band at 3441  $\text{cm}^{-1}$  is assigned to -OH group, the small peaks at 2918 and 2857  $\text{cm}^{-1}$  are due to the vibration of -CH<sub>2</sub> groups, the peaks at 1608 and 1763  $\text{cm}^{-1}$  are due to the stretching vibration of C=O groups in carboxylic moiety, the 1439  $\text{cm}^{-1}$  peak is due to C-OH or C-H stretching vibration, and the 1128  $\text{cm}^{-1}$  peak can be assigned to C-O stretching vibration [47]. After the hydrothermal treatment in ammonia, the bands at 2918, 2857, 1763  $\text{cm}^{-1}$  disappear while the C-O stretching peak around 1100  $\text{cm}^{-1}$  still exists. New peaks at 1614, 1384 and 3153  $\text{cm}^{-1}$  are assigned to C=O



**Fig. 6** – UV-Vis absorption spectra, and PL spectra of CQDs (a) and N-CQDs (b) aqueous solutions at different excitation wavelengths and their photographs (inset) excited by a 365 nm UV lamp. (A color version of this figure can be viewed online.)

stretching vibration, C=N/C–N and N–H in-plane stretching vibrations of amine groups [16,48], indicating the doping of nitrogen in N-CQDs. Both CQDs and N-CQDs are rich of hydrophilic groups such as carboxyl and hydroxyl groups that are formed in the chemical oxidation step of petroleum coke in concentrated  $\text{H}_2\text{SO}_4$  and  $\text{HNO}_3$ . The abundant hydrophilic groups help to greatly improve aqueous solubility of the CQDs, which are beneficial for the applications of the CQDs in fields such as biochemistry, diagnostics and drug delivery.

All of the results presented above including TEM, AFM, XRD, Raman, XPS and FT-IR results have confirmed that N-CQDs with more defects have been prepared by the hydrothermal treatment in ammonia. N-CQDs with a uniform size and diversity surface groups show an improved optical properties than the untreated CQDs, as discussed below.

### 3.4. Optical properties of CQDs and N-CQDs

The optical properties of CQDs and N-CQDs are measured by UV-Vis absorption and PL spectroscopy. Fig. 6a is the UV-Vis spectrum of as-prepared CQDs, showing an absorption band at 228 nm that can be attributed to  $\pi$ - $\pi^*$  electron transition of graphitic  $\text{sp}^2$  domains. This result is consistent with GQDs prepared by the electrolysis of graphite rod [34]. Fig. 6b is the UV-Vis spectrum of N-CQDs, with no obvious absorption band. A broad and weak absorption shoulder peak in the range of 250–420 nm can also be seen in Fig. 6a and b, which may be due to the  $n$ - $\pi^*$  transition of C–O or C–N groups in CQDs and N-CQDs [49,50].

It is known that the optical properties of CQDs and N-CQDs are related to their concentration in the solution to some degree. Slight blue-shifts can be observed in the maximum emission wavelengths of CQDs and N-CQDs when the aqueous solutions were gradually diluted (Fig. S3), which is due to the reduced particle aggregation of CQDs and N-CQDs in the diluted solutions, leading to higher band gaps [51]. The self-quenching phenomena take place in high concentration due to the aggregation quenching effect resulted from the stacking of polyaromatic structures.

Fig. 6 also shows the fluorescence emission spectra of CQDs and N-CQDs, which were measured at different excitation wavelengths with the concentrations being optimized. The CQDs excited at 340 nm UV light show strong yellow PL

centering at 510 nm (Fig. 6a). When the excitation wavelength increases from 320 to 580 nm, the PL peaks correspondingly red-shift from 480 to 600 nm. The excitation-dependent PL behavior of the CQDs is similar to the CQDs reported in literature [17,48,52,53]. The excitation-dependent emission may be associated with the aromatic C=C bonds and surface defects resulted from C–OH and C=O groups in the CQDs [49,52–54].

To explore the PL mechanism of CQDs, quantum confinement effects and the surface functional groups should be addressed here. It is known that the as-made CQDs have narrow particle distributions, abundant  $\text{sp}^2$  structures as well as hydroxyl and carboxyl moieties on their surface, which act as energy traps that make CQDs exhibit strong fluorescence.

In the case of N-CQDs, an excellent blue PL at UV light was observed, as shown in Fig. 6b. Despite the excitation wavelength increasing from 320 to 400 nm, the maximum emission wavelength of N-CQDs remains at 475 nm, which may be due to a new kind of surface state resulted from the doped nitrogen atoms [35]. As the excitation wavelength further increases to 520 nm, the maximum emission wavelength shows a red-shift from 480 to 540 nm. The corresponding PL excitation (PLE) spectrum of N-CQDs (475 nm) shows a blue-shift compared to that of CQDs (510 nm) (Fig. S4). It should be noted that the as-made CQDs and N-CQDs solutions are transparent, and exhibit strong PL even after 6 months in air at RT, indicating good fluorescent stability.

The optical performance of N-CQDs is affected by the amount of N content, and it can be tuned from blue to the greenish yellow region through decreasing amount of doped nitrogen, which can be confirmed in Table S2, Figs. S5 and S6. The level of doped nitrogen can be easily controlled by changing the hydrothermal temperature (Fig. S5), and this is consistent with the literature [31].

The PL properties of CQDs and N-CQDs in aqueous solutions are partly related to the pH value of the solutions. Fig. 7a shows the variation trend of the CQDs from petroleum coke. For CQDs, the PL intensity increases significantly as the pH increases from 2 to 5, then levels off in a neutral range with the pH from 5 to 9, and drops quickly in strong alkaline solution with the pH increasing from 9 to 12 (Fig. S7a). Because of this, the maximum emission wavelength red shifts from 493 to 509 nm as the pH decreases (Fig. S7b). This

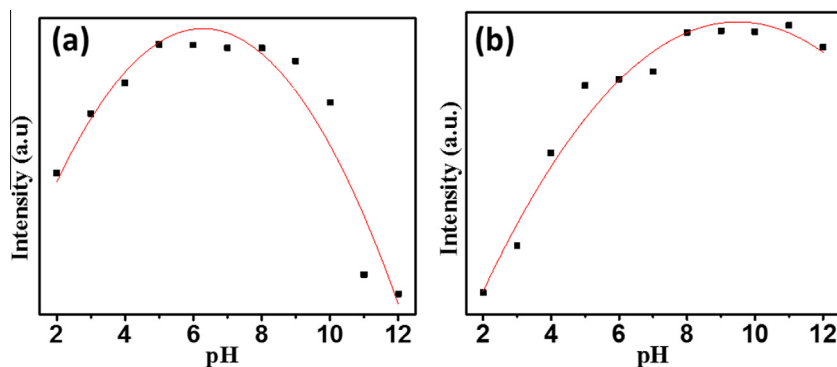


Fig. 7 – Effect of pH value on the PL intensity of CQDs (a) and N-CQDs (b) ( $\lambda_{\text{ex}} = 350 \text{ nm}$ ). (A color version of this figure can be viewed online.)

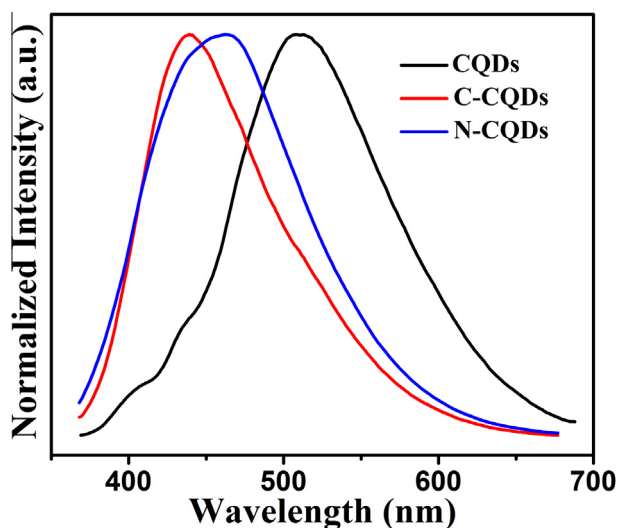


Fig. 8 – PL spectra of CQDs, C-CQDs and N-CQDs ( $\lambda_{\text{ex}} = 350 \text{ nm}$ ). (A color version of this figure can be viewed online.)

is due to the narrowed band gap resulted from the reduced deprotonation effect of carboxyl groups from high to low in pH value [17].

In the case of N-CQDs (Fig. 7b), the variation trend of the PL intensity differs from the CQDs as discussed before, which increases gradually as the pH increases from 2 to 8, then levels off in a range of pH from 8 to 12 (Fig. S7c). Because of this, the maximum emission wavelength of N-CQDs remains at 475 nm with the pH at 6–12 (Fig. S7d). This strong and stable PL of N-CQDs can be attributed to the amide groups on the surface of N-CQDs, which make the N-CQDs have a stable surface chemistry in neutral and alkaline conditions [55]. It should be noted that at pH below 5, the emission spectra of N-CQDs blue shift, with the PL intensity drops gradually as the pH decreases. Anyway, the fluorescence emission of N-CQDs solution can be easily tuned by adjusting the pH, which may be a protonation-driven effect in acid solutions [56]. It is believed that the pH-sensitive fluorescence property of CQDs and N-CQDs will be helpful to their applications in the field of pH-sensitive molecular sensing.

The obvious difference in the PL behaviors of CQDs and N-CQDs is closely related to the PL enhancement after the nitrogen doping, in which the mechanism involved needs to be addressed.

The role of doped nitrogen atoms in N-CQDs might be reorganized, leading to new surface states of CQDs, which further results in an efficient radiative recombination [46]. A complex heteroaromatic  $\pi$  system may be resulted from the nitrogen doping in CQDs [57]. In order to figure out the mechanism involved in this system, the as-obtained CQDs were treated by the same hydrothermal procedure in the absence of ammonia, yielding CQDs (termed as C-CQDs). Fig. 8 shows the PL spectra of CQDs, C-CQDs and N-CQDs, showing clearly that the maximum emission wavelength changes from 510 nm of the untreated CQDs to 440 nm of C-CQDs. The average size of C-CQDs is 1.6 nm (Fig. S8), which is much smaller than those of CQDs and N-CQDs (Fig. 2). The HRTEM of C-CQDs is given in Fig. S8. The lattice space of C-CQDs is 0.341 nm, indicating C-CQDs have certain crystallinity. This means that the hydrothermal treatment helps to tune CQDs to smaller size with an enhanced quantum confinement effect. It is noted that N-CQDs show much stronger PL intensity than C-CQDs excited at 365 nm. The QY of C-CQDs is 5.6%, which is much lower than 15.8% of N-CQDs (Table S1). The low PL quantum yield of C-CQDs is most probably ascribed to the fluorescence quenching caused by the aggregation of carbon dots without doped nitrogen. With the formation of the differences in particle size and surface functional groups between CQDs and N-CQDs, it is possible for one to assume that the strong blue emission of N-CQDs is related to two factors. First, new amide-containing fluorophores may be formed in the hydrothermal treatment in ammonia [50]. Second, the optical band gap of N-CQDs increases with decreasing  $sp^2$  domain size due to the quantum confinement effects [58]. Finally, a synergistic effect due to the combined contribution from the doped nitrogen atoms and size effect results in an improved PL properties of N-CQDs.

Based on the results discussed above, a schematic mechanism for fluorescence of CQDs and N-CQDs made from petroleum coke is proposed (Fig. 9). The CQDs with larger particle size and less surface states have a relative wide distribution of energy levels in comparison to the N-CQDs, showing an

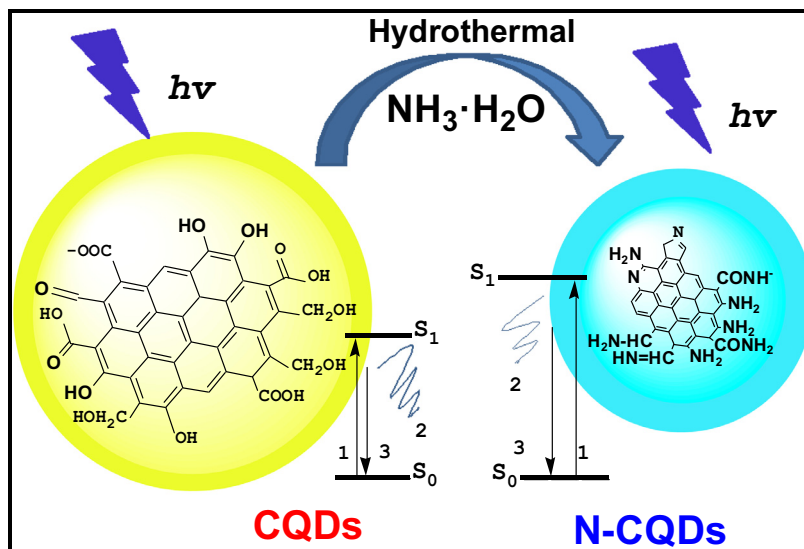


**Fig. 9** – Schematic for fluorescence mechanism of CQDs and N-CQDs. (1) electrons excited from the ground state ( $S_0$ ) and trapped by the surface excited states ( $S_1$ ); (2) excited electrons return to  $S_0$  via a non-radiative route; (3) excited electrons return to  $S_0$  via a radiative route. (A color version of this figure can be viewed online.)

excitation-dependent emission behavior and a relative weak PL signal. For the concerned CQDs and N-CQDs in the present work, a quantum confinement of emissive energy traps exist [53], i.e., a large surface-to-volume ratio is necessary for the passivated nanoparticles to exhibit strong photoluminescence. The nitrogen bonding to carbon may cause disorder in the carbon hexagonal rings and create new luminescent centers by trapping the radiative electron-hole pairs. As N-CQDs are enriched with primary amine, which can act as the electron-donating groups to enhance the conjugation degree of conjugated systems [59]. In a word, the doped nitrogen, the adsorbed primary amine [31] at the edges of N-CQDs, and the varied size of the  $sp^2$  domains all contribute to narrowed optical band gaps of N-CQDs with blue-shift in the PL emission. The radiative recombination of excitons [53,60]

between the delocalized  $\pi$  orbital and the doped nitrogen atoms in N-CQDs results in high photoluminescent QY, i.e. 15.8%, which is much higher than 8.7% of CQDs. The time decay of N-CQDs is 6.11 ns, much longer than 3.86 ns of CQDs (Fig. 10), which is agree with the PL enhancement.

The PL performance of CQDs and N-CQDs made from petroleum coke can be further improved by optimizing the preparation process, for example, by electrochemical and plasma treatments of the coke, and by co-doping other non-carbon atoms such as B/P/S in the matrix of CQDs. The work is in progress now, and the results will be reported soon.

#### 4. Summary

In sum, water-soluble photoluminescent CQDs are produced from petroleum coke for the first time by ultrasonic-assisted chemical oxidation method. The as-made CQDs and N-CQDs with graphene-like structures are rich of oxygen-containing functional groups, and have a uniform size and good dispersion, and excellent water solubility. Both CQDs and N-CQDs are sensitive to pH in a wide range of 2.0–12.0, and have a high QY. The QY of N-CQDs is 15.8%, much higher than 8.7% of the CQDs without N-doping by hydrothermal treatment in ammonia. This work offers a new way for producing high quality and tunable PL CQDs from petroleum coke.

#### Acknowledgements

This work was partly supported by the NSFC of China (Nos. 51372028, 21302224, 51372277); the Fundamental Research Funds for the Central Universities (14CX02060A, 13CX02066A). The authors wish to thank Prof. Zhenhui Kang and Prof. Yang Liu at Soochow University of China for fruitful discussion and Dr. Xiaojuan Wang at China University of Petroleum for assistance in AFM and PL analyses.

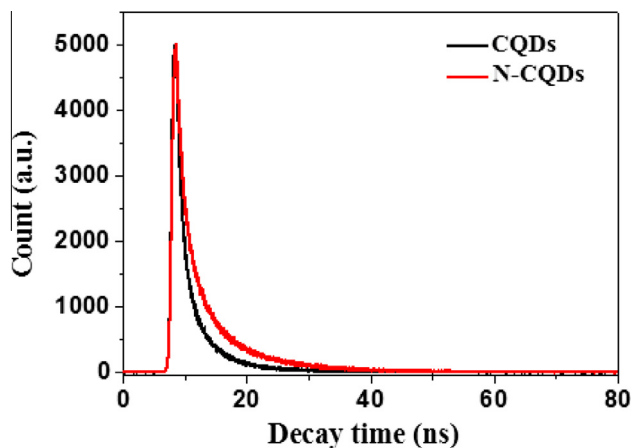


**Fig. 10** – Time-correlated single-photon counting of CQDs and N-CQDs. (A color version of this figure can be viewed online.)

## Appendix A. Supplementary data

Supplementary data associated with this article can be found, in the online version, at <http://dx.doi.org/10.1016/j.carbon.2014.07.029>.

## REFERENCES

- [1] Xu X, Ray R, Gu Y, Ploehn HJ, Gearheart L, Raker K, et al. Electrophoretic analysis and purification of fluorescent single-walled carbon nanotube fragments. *J Am Chem Soc* 2004;126(40):12736–7.
- [2] Kim S, Hwang SW, Kim MK, Shin DY, Shin DH, Kim CO, et al. Anomalous behaviors of visible luminescence from graphene quantum dots: interplay between size and shape. *ACS Nano* 2012;6(9):8203–8.
- [3] Yang F, Zhao M, Zheng B, Xiao D, Wu L, Guo Y. Influence of pH on the fluorescence properties of graphene quantum dots using ozonation pre-oxide hydrothermal synthesis. *J Mater Chem* 2012;22(48):25471–9.
- [4] Li L, Wu G, Yang G, Peng J, Zhao J, Zhu JJ. Focusing on luminescent graphene quantum dots: current status and future perspectives. *Nanoscale* 2013;5(10):4015–39.
- [5] Liu WW, Feng YQ, Yan XB, Chen JT, Xue QJ. Superior micro-supercapacitors based on graphene quantum dots. *Adv Funct Mater* 2013;23(33):4111–22.
- [6] Eda G, Lin YY, Mattevi C, Yamaguchi H, Chen HA, Chen I, et al. Blue photoluminescence from chemically derived graphene oxide. *Adv Mater* 2010;22(4):505–9.
- [7] Loh KP, Bao Q, Eda G, Chhowalla M. Graphene oxide as a chemically tunable platform for optical applications. *Nat Chem* 2010;2(12):1015–24.
- [8] Pan D, Zhang J, Li Z, Wu M. Hydrothermal route for cutting graphene sheets into blue-luminescent graphene quantum dots. *Adv Mater* 2010;22(6):734–8.
- [9] Liu F, Jang MH, Ha HD, Kim JH, Cho YH, Seo TS. Facile synthetic method for pristine graphene quantum dots and graphene oxide quantum dots: origin of blue and green luminescence. *Adv Mater* 2013;25(27):3657–62.
- [10] He W, Lu L. Revisiting the structure of graphene oxide for preparing new-style graphene-based ultraviolet absorbers. *Adv Funct Mater* 2012;22(12):2542–9.
- [11] Lu J, Yeo PSE, Gan CK, Wu P, Loh KP. Transforming C<sub>60</sub> molecules into graphene quantum dots. *Nat Nanotechnol* 2011;6(4):247–52.
- [12] Peng J, Gao W, Gupta BK, Liu Z, Romero Aburto R, Ge L, et al. Graphene quantum dots derived from carbon fibers. *Nano Lett* 2012;12(2):844–9.
- [13] Li H, He X, Liu Y, Huang H, Lian S, Lee ST, et al. One-step ultrasonic synthesis of water-soluble carbon nanoparticles with excellent photoluminescent properties. *Carbon* 2011;49(2):605–9.
- [14] Xu J, Zhou Y, Liu S, Dong M, Huang C. Low-cost synthesis of carbon nanodots from natural products as fluorescent probe for the detection of ferrum (III) ion in lake water. *Anal Methods* 2014;6(7):2086–90.
- [15] Liang Q, Ma W, Shi Y, Li Z, Yang X. Easy synthesis of highly fluorescent carbon quantum dots from gelatin and their luminescent properties and applications. *Carbon* 2013;60:421–8.
- [16] Sun D, Ban R, Zhang PH, Wu GH, Zhang JR, Zhu JJ. Hair fiber as a precursor for synthesizing of sulfur-and nitrogen-co-doped carbon dots with tunable luminescence properties. *Carbon* 2013;64:424–34.
- [17] Jia X, Li J, Wang E. One-pot green synthesis of optically pH-sensitive carbon dots with upconversion luminescence. *Nanoscale* 2012;4(18):5572–5.
- [18] Wu M, Zha Q, Qiu J, Han X, Guo Y, Li Z, et al. Preparation of porous carbons from petroleum coke by different activation methods. *Fuel* 2005;84(14):1992–7.
- [19] Liu H, Ye T, Mao C. Fluorescent carbon nanoparticles derived from candle soot. *Angew Chem Int Ed* 2007;46(34):6473–5.
- [20] Rahy A, Zhou C, Zheng J, Park S, Kim MJ, Jang I, et al. Photoluminescent carbon nanoparticles produced by confined combustion of aromatic compounds. *Carbon* 2012;50(3):1298–302.
- [21] Tang L, Ji R, Cao X, Lin J, Jiang H, Li X, et al. Deep ultraviolet photoluminescence of water-soluble self-passivated graphene quantum dots. *ACS Nano* 2012;6(6):5102–10.
- [22] Wang J, Wang CF, Chen S. Amphiphilic egg-derived carbon dots: rapid plasma fabrication, pyrolysis process, and multicolor printing patterns. *Angew Chem Int Ed* 2012;124(37):9431–5.
- [23] Li H, He X, Kang Z, Huang H, Liu Y, Liu J, et al. Water-soluble fluorescent carbon quantum dots and photocatalyst design. *Angew Chem Int Ed* 2010;49(26):4430–4.
- [24] Qiao ZA, Wang Y, Gao Y, Li H, Dai T, Liu Y, et al. Commercially activated carbon as the source for producing multicolor photoluminescent carbon dots by chemical oxidation. *Chem Commun* 2010;46(46):8812–4.
- [25] Tian L, Ghosh D, Chen W, Pradhan S, Chang X, Chen S. Nanosized carbon particles from natural gas soot. *Chem Mater* 2009;21(13):2803–9.
- [26] Shen J, Zhu Y, Yang X, Li C. Graphene quantum dots: emergent nanolights for bioimaging, sensors, catalysis and photovoltaic devices. *Chem Commun* 2012;48(31):3686–99.
- [27] Yang YH, Cui JH, Zheng MT, Hu CF, Tan SZ, Xiao Y, et al. One-step synthesis of amino-functionalized fluorescent carbon nanoparticles by hydrothermal carbonization of chitosan. *Chem Commun* 2012;48(3):380–2.
- [28] Liao B, Long P, He B, Yi S, Ou B, Shen S, et al. Reversible fluorescence modulation of spiropyran-functionalized carbon nanoparticles. *J Mater Chem C* 2013;1(23):3716–21.
- [29] Ayala P, Arenal R, Loiseau A, Rubio A, Pichler T. The physical and chemical properties of heteronanotubes. *Rev Mod Phys* 2010;82(2):1843.
- [30] Zhai X, Zhang P, Liu C, Bai T, Li W, Dai L, et al. Highly luminescent carbon nanodots by microwave-assisted pyrolysis. *Chem Commun* 2012;48(64):7955–7.
- [31] Tetsuka H, Asahi R, Nagoya A, Okamoto K, Tajima I, Ohta R, et al. Optically tunable amino-functionalized graphene quantum dots. *Adv Mater* 2012;24(39):5333–8.
- [32] Jin SH, Kim DH, Jun GH, Hong SH, Jeon S. Tuning the photoluminescence of graphene quantum dots through the charge transfer effect of functional groups. *ACS Nano* 2013;7(2):1239–45.
- [33] Liu Y, Wu P. Graphene quantum dot hybrids as efficient metal-free electrocatalyst for the oxygen reduction reaction. *ACS Appl Mater Interfaces* 2013;5(8):3362–9.
- [34] Zhang M, Bai L, Shang W, Xie W, Ma H, Fu Y, et al. Facile synthesis of water-soluble, highly fluorescent graphene quantum dots as a robust biological label for stem cells. *J Mater Chem* 2012;22(15):7461–7.
- [35] Dong Y, Pang H, Yang HB, Guo C, Shao J, Chi Y, et al. Carbon-based dots co-doped with nitrogen and sulfur for high quantum yield and excitation-independent emission. *Angew Chem Int Ed* 2013;52(30):7800–4.
- [36] Feng L, Liu YW, Tang XY, Piao Y, Chen SF, Deng SL, et al. Propagative exfoliation of high quality graphene. *Chem Mater* 2013;25(22):4487–96.

- [37] Zhou J, Yang Y, Zhang CY. A low-temperature solid-phase method to synthesize highly fluorescent carbon nitride dots with tunable emission. *Chem Commun* 2013;49(77):8605–7.
- [38] Hu C, Liu Y, Yang Y, Cui J, Huang Z, Wang Y, et al. One-step preparation of nitrogen-doped graphene quantum dots from oxidized debris of graphene oxide. *J Mater Chem B* 2013;1(1):39–42.
- [39] Li J, Lin H, Yang Z, Li J. A method for the catalytic reduction of graphene oxide at temperatures below 150 °C. *Carbon* 2011;49(9):3024–30.
- [40] Li Y, Zhao Y, Cheng H, Hu Y, Shi G, Dai L, et al. Nitrogen-doped graphene quantum dots with oxygen-rich functional groups. *J Am Chem Soc* 2011;134(1):15–8.
- [41] Fang Y, Guo S, Li D, Zhu C, Ren W, Dong S, et al. Easy synthesis and imaging applications of cross-linked green fluorescent hollow carbon nanoparticles. *ACS Nano* 2011;6(1):400–9.
- [42] Lu J, Yang JX, Wang J, Lim A, Wang S, Loh KP. One-pot synthesis of fluorescent carbon nanoribbons, nanoparticles, and graphene by the exfoliation of graphite in ionic liquids. *ACS Nano* 2009;3(8):2367–75.
- [43] Flatt AK, Chen B, Tour JM. Fabrication of carbon nanotube-molecule-silicon junctions. *J Am Chem Soc* 2005;127(25):8918–9.
- [44] Štengl V, Bakardjieva S, Henych J, Lang K, Kormunda M. Blue and green luminescence of reduced graphene oxide quantum dots. *Carbon* 2013;63:537–46.
- [45] Liu S, Tian J, Wang L, Zhang Y, Qin X, Luo Y, et al. Hydrothermal treatment of grass: a low-cost, green route to nitrogen-doped, carbon-rich, photoluminescent polymer nanodots as an effective fluorescent sensing platform for label-free detection of Cu (II) ions. *Adv Mater* 2012;24(15):2037–41.
- [46] Xu Y, Wu M, Liu Y, Feng XZ, Yin XB, He XW, et al. Nitrogen-doped carbon dots: a facile and general preparation method, photoluminescence investigation, and imaging applications. *Chem A Eur J* 2013;19(7):2276–83.
- [47] Liu L, Li Y, Zhan L, Liu Y, Huang C. One-step synthesis of fluorescent hydroxyls-coated carbon dots with hydrothermal reaction and its application to optical sensing of metal ions. *Sci China Chem* 2011;54(8):1342–7.
- [48] Jiang J, He Y, Li S, Cui H. Amino acids as the source for producing carbon nanodots: microwave assisted one-step synthesis, intrinsic photoluminescence property and intense chemiluminescence enhancement. *Chem Commun* 2012;48(77):9634–6.
- [49] Li M, Cushing SK, Zhou X, Guo S, Wu N. Fingerprinting photoluminescence of functional groups in graphene oxide. *J Mater Chem* 2012;22(44):23374–9.
- [50] Li W, Zhang Z, Kong B, Feng S, Wang J, Wang L, et al. Simple and green synthesis of nitrogen-doped photoluminescent carbonaceous nanospheres for bioimaging. *Angew Chem Int Ed* 2013;52(31):8151–5.
- [51] Hong Y, Lam JW, Tang BZ. Aggregation-induced emission: phenomenon, mechanism and applications. *Chem Commun* 2009;29:4332–53.
- [52] Zhu S, Zhang J, Tang S, Qiao C, Wang L, Wang H, et al. Surface chemistry routes to modulate the photoluminescence of graphene quantum dots: from fluorescence mechanism to up-conversion bioimaging applications. *Adv Funct Mater* 2012;22(22):4732–40.
- [53] Liu R, Wu D, Liu S, Koynov K, Knoll W, Li Q. An aqueous route to multicolor photoluminescent carbon dots using silica spheres as carriers. *Angew Chem Int Ed* 2009;121(25):4668–71.
- [54] Dong Y, Chen C, Lin J, Zhou N, Chi Y, Chen G. Electrochemiluminescence emission from carbon quantum dot-sulfite coreactant system. *Carbon* 2013;56:12–7.
- [55] Wang Y, Dong L, Xiong R, Hu A. Practical access to bandgap-like N-doped carbon dots with dual emission unzipped from PAN@ PMMA core-shell nanoparticles. *J Mater Chem C* 2013;1(46):7731–5.
- [56] Chen JL, Yan XP. Ionic strength and pH reversible response of visible and near-infrared fluorescence of graphene oxide nanosheets for monitoring the extracellular pH. *Chem Commun* 2011;47(11):3135–7.
- [57] Kozák OE, Datta KKR, Greplová M, Ranc V, Kašlík J, Zbořil R. Surfactant-derived amphiphilic carbon dots with tunable photoluminescence. *J Phys Chem C* 2013;117(47):24991–6.
- [58] Chang H, Sun Z, Saito M, Yuan Q, Zhang H, Li J, et al. Regulating infrared photo responses in reduced graphene oxide phototransistors by defect and atomic structure control. *ACS Nano* 2013;7(7):6310–20.
- [59] Ding H, Zhang P, Wang TY, Kong JL, Xiong HM. Nitrogen-doped carbon dots derived from polyvinyl pyrrolidone and their multicolor cell imaging. *Nanotechnology* 2014;25(20):205604.
- [60] Wang Q, Wang W, Lei J, Xu N, Gao F, Ju H. Fluorescence quenching of carbon nitride nanosheet through its interaction with DNA for versatile fluorescence sensing. *Anal Chem* 2013;85(24):12182–8.